One-Equation Turbulence Model for Transonic Airfoil Flows

R. A. Mitcheltree*
North Carolina State University, Raleigh, North Carolina
M. D. Salas†
NASA Langley Research Center, Hampton, Virginia
and
H. A. Hassan‡
North Carolina State University, Raleigh, North Carolina

A one-equation turbulence model based on the turbulent kinetic energy equation is presented. The model is motivated by the success of the Johnson-King model and is developed from the available experimental observations on both attached and separated turbulent flows. Results for both attached and separated flow about the NACA 0012 and RAE 2822 airfoils are compared with the Baldwin-Lomax algebraic turbulence model, the q-ω two-equation model, the Johnson-King model, and available experimental pressure and skin-friction data. Based on the results obtained, the model duplicates the success of algebraic models in attached-flow cases. For separated-flow cases, it predicts shock location and strength closer to the experimentally observed values than both the algebraic and two-equation models. However, the model suffers some limitations in predicting shock location for transonic cases with large shock-induced separation.

Introduction

IT is generally accepted that algebraic turbulence models are not suited to describe nonequilibrium turbulent flows.[1] A nonequilibrium turublent flow is defined as a flow in which the so-called "history" effects of convection and diffusion of turbulent energy are sufficiently strong to upset the balance between local production and dissipation of turbulence. Separation on transonic airfoils is an example of such a flow.

Since the algebraic models are inadequate for these complex flows, the next step is to use a higher-order closure model. Unfortunately, the work of Patel et al.[2] showed that most of the k-ε models and related two-equation models lack generality since they are unable to predict some well-documented features of simple shear flows. Moreover, the work of Coakley[3] showed that, in the presence of separation, predictions of existing two-equation models are not much better than the predictions of the algebraic models.

The model of Johnson and King,[4] which is based on a simplified version of the turbulent kinetic energy equation, performs well in regions where nonequilibrium turbulent effects are important. However, it does not always perform well in regions where equilibrium turbulent flow exists. The success of this model suggests that the turbulent kinetic energy equation migh' contain sufficient physics to model separated flows.

Because of the preceding, an effort is undertaken to develop a new one-equation turbulence model based on the turbulent kinetic energy equation. The model is developed directly from the available experimental observations of both attached and separated flows. It consists of three elements: an attached-flow formulation, a separated-flow formulation, and an automatic blending which smoothly switches between the two formulations. This blending function is based on an experimentally observed indicator of separation. The model does not require prior knowledge of separation or its location.

For a one-equation turbulence model, closure of the governing equations simplifies to specification of the turbulent length scales. The attached-flow formulation defines these length scales to recover the logarithmic law-of-the-wall velocity profiles. Most of the previous work using one-equation models used the same length scale for turbulent stresses and turbulent dissipation while employing a near-wall adjustment of the eddy viscosity to account for low-Reynolds-number effects. Many of these models suffered numerical difficulties in the near-wall region and required adjustment to handle different flows. The present one-equation model defines two different length scales, one for the turbulent stresses and one for turbulent dissipation. For attached flows, the two length scales are identical everywhere except in the very near wall region. In this region, specification of the length scales requires close attention to near-wall scaling. In addition, the present one-eqation model eliminates the need to find the edge of the boundary layer when defining outer-layer length scales. A function based on vorticity which was used by Baldwin and Lomax[5] is used to define the outer-layer length scale.

To handle separated flows, the model incorporates features uncovered by experimental investigations of separated flows. Simpson[1] observed that the logarithmic law-of-the-wall relations do not describe the velocity profile for separated boundary layers. In fact, scaling within and outside separated flow regions is not the same. Although attached turbulent flows can be scaled with respect to wall-friction velocity, this quantity is zero at a mean flow-separation point. Simpson observed that separated flows are scaled with respect to maximum shear stress and its location as the characteristic velocity and length scales. At present, no similarity relations have emerged which describe the entire velocity profile for separated regions. However, the Schofield-Perry velocity profiles[6] have been shown to approximate the forward flow profiles for strong adverse pressure gradient and separated boundary layers. These profiles correctly use the maximum

Received April 14, 1989; revision received Sept. 25, 1989.

*Currently Aerospace Technologist, Aerothermodynamics Branch, Space Systems Division, NASA Langley Research Center, Hampton, VA. Member AIAA.

†Professor, Mechanical and Aerospace Engineering. Associate Fellow AIAA.

‡Head, Theoretical Aerodynamics Branch, Transonic Aerodynamics Division. Associate Fellow AIAA.

Reynolds shear stress and its location as the characteristic velocity and length scales. Thus, in the same manner in which the attached-flow formulation defines its length scales to recover the law-of-the-wall profiles, the separated-flow formulation defines its length scales to recover the Schofield-Perry velocity profiles.

Simpson made two additional observations which are incorporated in the present model. He finds that the ratio of Reynolds shear stress to turbulent kinetic energy, called the turbulent structural coefficient, decreases in the presence of separation.

His final observation on separated turbulent flows concerns the unsteadiness of such flows. As detachment is approached, near-wall mean velocity components become smaller. Turbulent fluctuations in the flowfield cause the instantaneous flow to spend an increasing amount of time in the backflow direction. Simpson defined a variable γ_{pu} as the fraction of time that the instantaneous flow moves downstream (positive u). For example, $\gamma_{pu} = 0.5$ implies that the instantaneous flow spends half of its time going downstream and half upstream. Thus, at such a point the mean velocity $\tilde{u}$ is near zero. Simpson established a correlation between γ_{pu} and the ratio of local mean streamwise velocity to turbulence intensity. This indicator of separation is utilized to automatically blend the attached-flow formulation and the separated-flow formulation.

The central-difference finite-volume Navier-Stokes code employed is based on that used by Swanson and Turkel.[7] The turbulent kinetic energy equation is coupled to the conservation equations and a four-stage Runge-Kutta time-stepping scheme is employed. The equations are integrated to the wall where the no-slip and zero turbulence energy boundary conditions are applied. The scheme uses a blended second- and fourth-difference numerical damping formulation. Normal direction damping is not used on the first four cells adjacent to a wall boundary. It is noted that Navier-Stokes codes which use the original Johnson-King model or higher-order closure models cannot be started from a uniform flow condition. The usual procedure is to use an initial solution obtained from a flow solver that incorporates an algebraic turbulence model. This inefficient starting procedure is not necessary in the present work.

Results for NACA 0012 and RAE 2822 airfoil flows are presented and compared with experimental data and other computational results.

Governing Equations

The equations governing turbulent mean flow past airfoils are the Reynolds-averaged conservation equations of mass, momentum, and energy and the turbulent kinetic energy equation. When Favre's mass-averaging and indicial notation are used, the conservation equations are[8]

$$\bar{\rho}_{,t} + (\bar{\rho}\tilde{u}_j)_{,j} = 0 \tag{1}$$

$$(\bar{\rho}\tilde{u}_i)_{,t} + [\bar{\rho}\tilde{u}_j\tilde{u}_i + \delta_{ij}\bar{P} - (\bar{\tau}_{ij} - \overline{\rho u_i'' u_j''})]_{,j} = 0 \tag{2}$$

$$(\bar{\rho}\tilde{E})_{,t} + [\tilde{u}_j(\bar{\rho}\tilde{E} + \bar{P}) + \bar{q}_j + \overline{\rho u_j'' h''}]_{,j} - [\tilde{u}_i(\bar{\tau}_{ij} - \overline{\rho u_i'' u_j''})]_{,j} = 0 \tag{3}$$

where

$$\bar{\tau}_{ij} = \mu\left[\tilde{u}_{i,j} + \tilde{u}_{j,i} - \frac{2}{3}\delta_{ij}\tilde{u}_{m,m}\right] \tag{4}$$

$$\bar{q}_j = -\lambda\tilde{T}_{,j} \tag{5}$$

$$\bar{P} = \bar{\rho}(\gamma - 1)\left[\tilde{E} - \frac{1}{2}\tilde{u}_i\tilde{u}_i\right] \tag{6}$$

where $\bar{\rho}$ is the density, $\tilde{u}_i$ is the mean velocity in the direction of x_i, $\tilde{E}$ and h are the total energy and enthalpy per unit mass, and $\bar{P}$ is the mean pressure. $\bar{T}$, μ, and λ are, respectively, the temperature and the coefficients of molecular viscosity and conductivity. Closure of the Reynolds-averaged equations requires specification of the Reynolds stresses and heat flux terms. In most turbulence models, the turbulent stresses and heat fluxes are determined from the eddy viscosity (Boussinesq) approximation:

$$\overline{\rho u_i'' u_j''} = -\mu_t\left[\left(\frac{\partial\tilde{u}_j}{\partial x_i} + \frac{\partial\tilde{u}_i}{\partial x_j}\right) - \frac{2}{3}\delta_{ij}\frac{\partial\tilde{u}_m}{\partial x_m}\right] + \frac{2}{3}\delta_{ij}\bar{\rho}\tilde{k} \tag{7}$$

$$\overline{\rho u_i'' h''} = -\frac{c_p\mu_t}{Pr_t}\left(\frac{\partial\tilde{h}}{\partial x_i}\right) \tag{8}$$

where Pr_t is the turbulent Prandtl number (generally $Pr_t = 1$), μ_t is the eddy viscosity, and $\tilde{k}$ is the mean turbulent kinetic energy per unit mass:

$$\bar{\rho}\tilde{k} = \frac{1}{2}\overline{\rho u_i'' u_i''} \tag{9}$$

The preceding eddy viscosity assumption assumes that the transport of flow properties due to the action of turbulent eddies is analogous to the transport of properties due to molecular interactions. Turbulence is then modeled as an effective increase in the transport coefficients.

The exact turbulent kinetic energy equation can be derived directly from the Reynolds-averaged equations. However, before the equation can be solved, model terms are required for turbulent diffusion, pressure diffusion, pressure work, and dissipation of turbulent kinetic energy. The modeled turbulent kinetic energy equation used here is a compressible form of the equation proposed by Launder et al. (model 2 of Ref. 9):

$$(\bar{\rho}\tilde{k})_{,t} + [\bar{\rho}\tilde{u}_j\tilde{k} - \nu(\bar{\rho}\tilde{k})_{,j}]_{,j} - \left[c_k\frac{\tilde{k}}{\bar{\epsilon}}\overline{\rho u_i'' u_j''}(\bar{\rho}\tilde{k})_{,i}\right]_{,j} = -\overline{\rho u_i'' u_j''}\tilde{u}_{i,j} - \bar{\rho}\epsilon \tag{10}$$

where c_k is a constant (0.1), ν the molecular kinematic viscosity. The ϵ is the turbulent kinetic energy dissipation rate:

$$\epsilon = \frac{\tilde{k}^{3/2}}{l_\epsilon} \tag{11}$$

where l_ϵ is the dissipation length scale. The steady terms in Eq. (10) from left to right are the convection, the molecular diffusion, the turbulent diffusion, the production, and the rate of dissipation of the turbulent kinetic energy. The pressure work and pressure diffusion terms of the exact k equation are not directly modeled in the preceding equation. Turbulent diffusion is modeled by a gradient-driven diffusion term which contains a tensor diffusion coefficient unlike the scalar coefficient used in most one-equation models.

In a one-equation turbulent model, the eddy kinematic viscosity is given by the Kolmogrov-Prandtl relation:

$$\nu_t = C_\mu\sqrt{\tilde{k}}l_\mu \tag{12}$$

where C_μ is a constant and l_μ is the turbulent length scale.

Closure of the Reynolds-averaged equations when a one-equation eddy viscosity turbulence model is employed reduces to the specification of the turbulent dissipation length scale l_ϵ and turbulent length scale l_μ.

Approach

First, a closure formulation (i.e., definitions of the length scales) is developed for attached flows noting all of the assumptions used in its development. Next, using the same methodology, a separated-flow formulation is developed using the available observations concerning separated flows. Fi-

nally, the automatic γ_{pu} switching function which smoothly blends the two formulations is discussed.

Attached-Flow Formulation

Closure of the Reynolds-averaged equations requires specification of the length scales l_ϵ and l_μ. The attached-flow formulation is developed by examining the incompressible attached turbulent flow over a flat plate. This methodology of affecting closure by examining one specific flow does not restrict the model's applicability to just that flow; rather it calibrates the model to handle a whole family of related flows.

The logarithmic law-of-the-wall relations describe the velocity profiles for attached turbulent flat-plate flow. Length scale definitions, denoted by an "a" superscript for the attached formulation, are described for the inner layer, the outer layer, and the viscous sublayer of the boundary layer. The inner layer is discussed first. In this region, the eddy viscosity assumption, Eq. (7), for the Reynolds shear stress becomes

$$-\overline{u''v''} = C_\mu \sqrt{\tilde{k}} l_\mu \frac{\partial \tilde{u}}{\partial y} \tag{13}$$

In this layer, the k equation, Eq. (10), simplifies to production equals dissipation:

$$-\overline{u''v''}\frac{\partial \tilde{u}}{\partial y} = \frac{\tilde{k}^{3/2}}{l_\epsilon} \tag{14}$$

Eliminating the mean velocity derivative from Eqs. (13) and (14) reveals that in this region $-u''v''/k$ is a constant:

$$C_\mu^2 = \left(\frac{-\overline{u''v''}}{\tilde{k}}\right) \tag{15}$$

This constant ratio, the turbulent structural coefficient, is experimentally observed to be 0.3 by Hinze.[10] Thus, the commonly used value $C_\mu = 0.09$ is set.

The velocity profile for the inner layer is defined by the log-law relation:

$$u^+ = \frac{1}{\kappa}\ell n y^+ + B \tag{16}$$

$$u^+ = \frac{u}{u_\tau} \tag{17}$$

$$y^+ = \frac{u_\tau y}{\nu} \tag{18}$$

where u_τ is the wall-friction velocity, $B = 5.5$, and $\kappa = 0.41$. Hence,

$$\frac{\partial \tilde{u}}{\partial y} = \frac{u_\tau}{\kappa y} \tag{19}$$

In addition, shear stress across the inner layer is assumed constant:

$$-\overline{u''v''} = u_\tau^2 \tag{20}$$

Combining Eqs. (13), (14), (19), and (20) defines the length scales for the inner layer of the attached model:

$$l_\epsilon^a = l_\mu^a = \kappa C_\mu^{-3/4} y \tag{21}$$

In the outer layer of the boundary layer, mixing-length theory suggests that the length scales are a constant proportional to the boundary-layer thickness δ. However, it is difficult to find δ numerically. Baldwin and Lomax developed a function $F(y)$ related to vorticity ω which has a well-defined maximum:

$$F(y) = |\omega| y \tag{22}$$

The height of this function's maximum is proportional to δ. Hence, in the outer layer the length scales are defined as

$$l_\epsilon^a = l_\mu^a = y_{F\max} \tag{23}$$

where $y_{F\max}$ is the value of y where $F(y)$ is a maximum. Specification of the length scales in the outer layer is not critical since in this region the convection terms begin to dominate the momentum and heat equations.

Correct treatment of the very near wall viscous sublayer is critical. Here the velocity profile is linear:

$$u^+ = y^+ \tag{24}$$

From the continuity equation and the no-slip boundary condition, it can be shown that $\tilde{k}$ varies like y^2 in the very near wall region. This causes the k equation to reduce to a balance between molecular diffusion and dissipation of $\tilde{k}$:

$$\nu \frac{\partial^2 k}{\partial y^2} = \frac{k^{3/2}}{l_\epsilon} \tag{25}$$

Since k varies as y^2,

$$\frac{\partial^2 k}{\partial y^2} = \frac{2k}{y^2} \tag{26}$$

Then,

$$l_\epsilon^a = \frac{\sqrt{k} y^2}{2\nu} \tag{27}$$

An exponential blending is used to combine the viscous sublayer and inner-layer dissipation length scale definitions into a single expression:

$$l_\epsilon^a = C_l y\left[1 - \exp\left(\frac{-R_e\sqrt{k}y}{2C_l}\right)\right] \tag{28}$$

$$C_l = \kappa C_\mu^{-3/4} \tag{29}$$

where R_e is the Reynolds number. Wolfstein[11] was the first to propose the use of two length scales with $l_\mu \neq l_\epsilon$ in the viscous sublayer. Chen and Patel[12] established the preceding exponential near-wall damping term which is based on $\sqrt{k}$ rather than the wall-friction velocity.

What is the turbulent length scale l_μ^a in the viscous sublayer? Analogous to Eq. (28), let

$$l_\mu^a = C_l y\left[1 - \exp\left(\frac{-R_e\sqrt{k}y}{A_\mu}\right)\right] \tag{30}$$

The value of A_μ can be determined by a number of different ways. Its value must be set correctly to recover the additive constant B in the log-law relations, Eq. (16). Consider mixing-length theory and the van Driest damping function:

$$-\overline{u''v''} = l^2 \left|\frac{\partial \tilde{u}}{\partial y}\right|\frac{\partial \tilde{u}}{\partial y} \tag{31}$$

$$l = \kappa y\left[1 - \exp\left(\frac{-y}{A}\right)\right] \tag{32}$$

$$A = \frac{26\nu}{u_\tau} \tag{33}$$

As $y \to 0$, Eq. (30) becomes

$$l_\mu^a = \frac{C_l R_e \sqrt{k} y^2}{A_\mu} \tag{34}$$

and Eq. (32) becomes

$$l = \frac{\kappa u_\tau y^2}{26\nu} \tag{35}$$

Equating the two eddy viscosities and utilizing Sirkan and Hanratty's experimental near-wall relation[2]

$$k = 0.05u_\tau^2 y^{+2} \tag{36}$$

yields the constant $A_\mu = 76$ (note: A_μ has units of velocity times length). The preceding value is used when properties are nondimensionalized with the velocity:

$$\left(\frac{P_\infty}{\rho_\infty}\right)^{1/2} \tag{37}$$

and the chord length c.

The complete attached formulation length scales can then be presented as

$$l_\epsilon^a = \min(L_\epsilon, y_{F\max}) \tag{38}$$

$$l_\mu^a = \min(L_\mu, y_{F\max}) \tag{39}$$

where

$$L_\epsilon = C_l y\left[1 - \exp\left(\frac{-R_e\sqrt{k}y}{2C_l}\right)\right]$$

$$L_\mu = C_l y\left[1 - \exp\left(\frac{-R_e\sqrt{k}y}{A_\mu}\right)\right] \tag{40}$$

The constants in the definition are

$$C_l = \kappa C_\mu^{-3/4}$$

$$C_\mu = 0.09$$

$$\kappa = 0.41$$

$$A_\mu = 76$$

In the wake region, the exponential near-wall damping term is eliminated from the length scale definitions.

In summary, the following assumptions were used in the development of the attached formulation. First, the eddy viscosity assumption was used to relate the Reynolds stresses and heat fluxes to the local strain rates of the mean flow. Next, the turbulent structural coefficient $\overline{-u''v''}/k$ was assumed to be 0.3. Finally, the logarithmic law of the wall relations were used to set the dissipatoin and turbulent length scales.

Separated-Flow Formulation

Development of the separated-flow formulation proceeds in the same manner as that for the attached flow. The differences between the two formulations are a direct result of experimentally observed differences between the respective flows.

For separated flow regions, Simpson observed that sufficiently far from the wall, where $\tilde{k} \geq 0.5\,\tilde{k}_m$ ($\tilde{k}_m$ is the maximum $\tilde{k}$ value),

$$\frac{-\overline{u''v''}}{k} = a = 0.2 \tag{41}$$

It is assumed that in the region where the preceding relation holds, the length scales vary linearly:

$$l_\epsilon^s = l_\mu^s = C_s y \tag{42}$$

To determine C_s, it is further assumed that at some point above where $\tilde{k} = 0.5\tilde{k}_m$ not only do the preceding two conditions hold but a balance between production and dissipation of turbulent kinetic energy exists and the Schofield-Perry[6] similarity relations hold.

The Schofield-Perry similarity describes the forward flow velocity profiles above the backflow region where the origin of the profile is displaced to the $\tilde{u} = 0$ line.

$$\frac{\tilde{u}}{U_1} = 0.47\left(\frac{U_s}{U_1}\right)^{3/2}\left(\frac{y'}{\delta^*}\right)^{1/2} + 1 - \frac{U_s}{U_1} \tag{43}$$

$$\frac{U_s}{U_m} = 8.0\left(\frac{B_{ps}}{L}\right) \tag{44}$$

$$B_{ps} = 2.86\delta^* \frac{U_1}{U_s} \tag{45}$$

$$U_m = \left(\frac{\tau_m}{\rho}\right)^{1/2} \tag{46}$$

Thus,

$$\frac{\partial\tilde{u}}{\partial y} = 2.458\left(\frac{\tau_m}{\rho}\right)^{3/8}\left(\frac{U_1\delta^*}{L^3}\right)^{1/4} y'^{-1/2} \tag{47}$$

where y' denotes the normal height above the $\tilde{u} = 0$ line, τ_m is the maximum shear stress, L the value of y' where $\tau = \tau_m$, δ^* the displacement thickness, and U_1 the edge velocity.

In order to calculate C_s, certain assumptions are made to cast Eq. (47) in terms of quantities that can be calculated readily. Using Eq. (41), τ_m is replaced by

$$\tau_m = a\tilde{k}_m \tag{48}$$

The quality L is then the value of y', where $\tilde{k} = \tilde{k}_m$. Analogous to the Baldwin-Lomax turbulence model, the product $\delta^* U_1$ is replaced with $(1.6y_{F\max}F_{\max})$ defined in Eq. (22). With these substitutions, Eq. (47) becomes

$$\frac{\partial\tilde{u}}{\partial y} = 2.458(a\tilde{k}_m)^{3/8}\left(\frac{1.6y_{F\max}F_{\max}}{L^3}\right)^{1/4} y'^{-1/2} \tag{49}$$

Combining Eqs. (14), (42), and (49) yields

$$C_s = \frac{\tilde{k}_m^{1/8} y'^{1/2} L^{3/4}}{2.9a^{11/8}(Y_{\max}F_{\max})^{1/4} y} \tag{50}$$

For a given x location, the point where the four conditions used in the C_s development simultaneously hold is between where $\tilde{k} = 0.5\tilde{k}_m$ and $\tilde{k} = \tilde{k}_m$. The results presented use $0.9\tilde{k}_m$. Numerical experiments show that C_s is not sensitive to the location when chosen within this range; C_s is, however, a function of x. This is one major difference between the separated formulation and the attached formulation where C_l was found to be a constant.

To complete the separated-flow formulation, length scales must be defined in the very near wall region and the outer layer. As in the attached case, definition of the dissipation length scale in the very near wall region requires a balance between molecular diffusion and turbulent dissipation of turbulent kinetic energy. Therefore a near-wall damping adjustment is still required of the same form as in Eq. (25). However, for the separated formulation the $2C_l$ in the denominator of the exponential term becomes $2C_s$.

The outer length scale is assumed to still be a constant proportional to the boundary-layer thickness. As before,

$$l_\epsilon^s = l_\mu^s = y_{F\max} \tag{51}$$

The length-scale definitions for the separated formulation are complete. They have identical form to the attached formulation, Eqs. (38) and (39), except that C_l is replaced with C_s. It remains to describe the manner in which the attached formulation is smoothly blended into the separated formulation using the blending function γ_{pu}.

Blending Function

As stated in the Introduction, $\gamma_{pu}(x,y)$ is a point function indicating the fraction of time local instantaneous flow proceeds in the downstream direction. Simpson[1] established a correlation between γ_{pu} and the ratio of mean streamwise velocity to turbulence intensity:

$$\gamma_{pu} = \frac{1}{2}\left[1 + \text{erf}\left(\frac{\tilde{u}}{2\sqrt{\overline{u''u''}}}\right)\right] \tag{52}$$

The correlation contains the error function erf. In the present numerical setting, a value of 3 in the error function argument proved a more appropriate value than the value recommended by Simpson. This discrepancy is a result of the eddy viscosity assumption which underpredicts the normal Reynolds stress $\overline{u''u''}$. From this point function, the degree of separation at each x/c station on the airfoil can be defined as the minimum value of γ_{pu} at that location. This new variable is denoted with a prime $\gamma'_{pu}(x)$ and, for all y, is defined as

$$\gamma'_{pu}(x) = \min\left[\gamma_{pu}(x,y)\right] \tag{53}$$

The $\gamma'_{pu} = 1$ indicates that the viscous layer is fully attached at that airfoil location; $\gamma'_{pu} \le 0.5$ indicates that mean backflow is present.

The use of γ'_{pu} to blend the attached-flow formulation and the separated-flow formulation is straightforward. In particular, only the attached-flow length scales are used when $\gamma'_{pu} = 1$ and only the separated-flow length scales are used when $\gamma'_{pu} \le 0.5$. For the intervening region, where $1.0 > \gamma'_{pu} > 0.5$, a linear combination of the respective length scales defines the blended length scales:

$$l_\epsilon = 2[(\gamma'_{pu} - 0.5)l^a_\epsilon + (1 - \gamma'_{pu})l^s_\epsilon] \tag{54}$$

$$l_\mu = 2[(\gamma'_{pu} - 0.5)l^a_\mu + (1 - \gamma'_{pu})l^s_\mu] \tag{55}$$

Because γ'_{pu} is a smoothly varying function, there is a smooth switch from attached-flow to separated-flow length scales.

Finally, it has been noted that the turbulent structural coefficient changes from 0.3 in attached regions to 0.2 in separated regions. The eddy viscosity coefficient defined in Eq. (12) contains the constant C_μ whose value was defined as the square root of the turbulent structural coefficient in Eq. (15). To remain consistent with experimental observations, the value of C_μ should decrease from 0.09 in attached region to 0.04 in separated regions. The $\gamma_{pu}(x,y)$ function facilitates this switch. The $C_\mu = 0.09$ when $\gamma_{pu} = 1$ and $C_\mu = 0.04$ when $\gamma_{pu} \le 0.5$. For $1.0 > \gamma_{pu} > 0.5$,

$$C_\mu = 2\{[\gamma_{pu}(x,y) - 0.5]0.09\} + 2\{[1 - \gamma_{pu}(x,y)]0.04\} \tag{56}$$

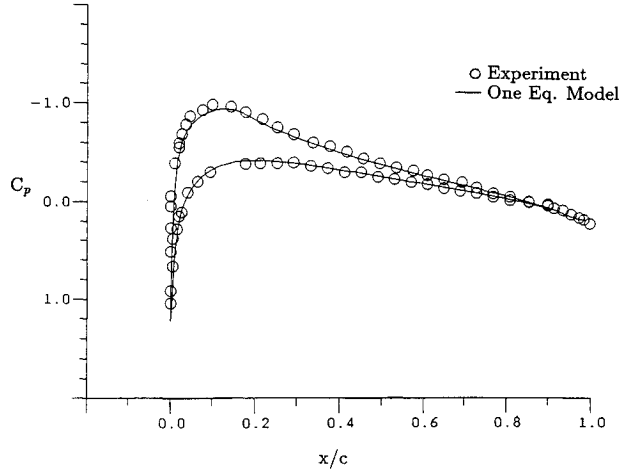

Fig. 1 Turbulent flow over an NACA 0012 airfoil ($M_\infty = 0.7$, $\alpha = 1.49$ deg, $R_e = 9 \times 10^6$): pressure distributions.

In summary, γ_{pu} and the attached length scales l^a_ϵ and l^a_μ are computed throughout the computational domain. The γ'_{pu} is then computed along the airfoil surface. In regions where $\gamma'_{pu} < 1$, the separated length scales l^s_ϵ and l^s_μ are computed and then blended with the attached lengths by Eqs. (54) and (55). Finally, the eddy velocity coefficient is computed using the blended C_μ value from Eq. (56).

Results and Discussion

The results presented here are for the NACA 0012 airfoil and the RAE 2822 airfoil. No adjustments are made to the turbulence model when different test cases are considered. Results are compared with experimental pressure and skin-friction data as well as Coakley's[3] computational results using an implicit upwind-difference scheme with the Baldwin-Lomax algebraic turbulence model, the q-ω two-equation model, and the Johnson-King model. Wind-tunnel corrections, as suggested by the experimenters using a linear-analysis technique, are utilized in establishing the computational angles of attack.

Flat-plate flow at zero angle of attack was considered first. Although not shown, excellent agreement of the velocity and skin-friction predictions with accepted correlations was realized. This result is not surprising since the attached-flow formulation of the turbulence model was calibrated by examining flat-plate flow.

The first airfoil case is attached flow about the NACA 0012 airfoil at $M_\infty = 0.7$, $\alpha = 1.49$ deg, and $R_e = 9 \times 10^6$. This calculation as well as the next employs a 160×79 C-grid. The normal spacing of the first point off the wall is 2×10^{-5}. The grid extends seven chord lengths in all directions. Figure 1 compares the computed pressure distribution of the present theory with the experiment of Ref. 13. As is seen in the figure, both upper and lower surface pressure distributions are well-predicted by the present one-equation model. The predicted life coefficient is 0.207. The experimental measured normal coefficient is 0.241.

A test case with large separation is $M_\infty = 0.799$, $R_e = 9 \times 10^6$ flow about the NACA 0012 airfoil at $\alpha = 2.26$ deg (corrected). This case is a severe test of the turbulence model. The calculation is performed on a 258×80 grid generated by a hyperbolic grid-generation method. The grid extent is 20 chords in all directions. The normal spacing of the first point off the wall is 2×10^{-5}. The present one-equation model was run for this case initially using only the attached-flow formulation. The resulting pressure distribution indicated an overprediction of shock location and strength like that of the algebraic Baldwin-Lomax and the two-equation q-ω models. Thus, when dealing with separated flows, it is not the number of equations used in describing the turbulence that is important but the physical model that the equations describe. There is a need for a model that is capable of first detecting separation and then describing it. Figure 2a compares the computed pressure distribution of the complete present model with the experimental data of Ref. 13 and Coakley's results using the Johnson-King model. The Johnson-King model accurately predicts the pressure distribution on the upper surface for this case. Figure 2b compares the computed pressure distribution with the experimental data and Coakley's results using the Baldwin-Lomax turbulence model and the two-equation q-ω model. The present one-equation model still predicts a shock location which is downstream of the experimental location, although not as far downstream as the algebraic and two-equation models. In addition, the present model now predicts the correct pressure plateau behind the shock. Both the present model and the Johnson-King model predict pressures on the lower surface of the airfoil lower than the experimental values. The smeared shock in the present results is due to inadequate grid resolution. Eighty cells are used on the upper surface of the airfoil. This grid is used to allow comparison with Coakley's results. Coakley[3] reports that a "typical" numerical grid used in his upwind-differenc-

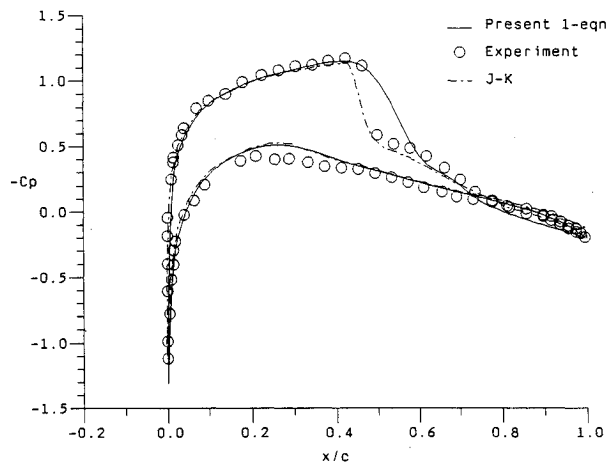

Fig. 2a Turbulent flow over an NACA 0012 airfoil ($M_\infty = 0.799$, $\alpha = 2.26$ deg (corrected), $R_e = 9 \times 10^6$): pressure distributions.

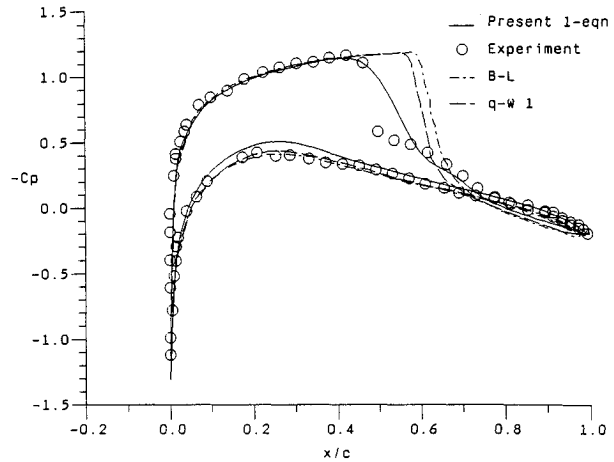

Fig. 2b Turbulent flow over an NACA 0012 airfoil ($M_\infty = 0.799$, $\alpha = 2.26$ deg (corrected), $R_e = 9 \times 10^6$): pressure distributions.

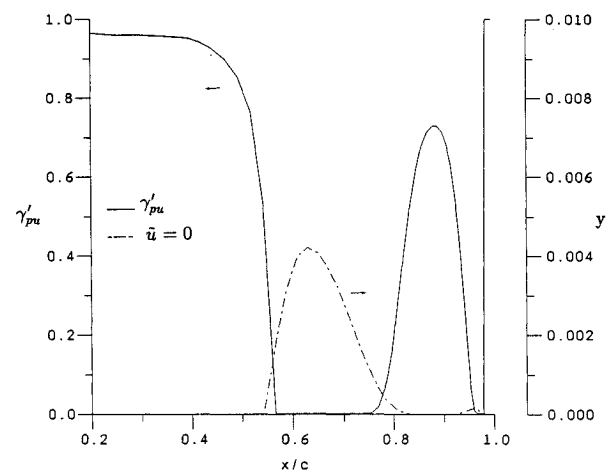

Fig. 3 The γ'_{pu} distribution and separation bubble extent for turbulent flow over an NACA 0012 airfoil [$M_\infty = 0.799$, $\alpha = 2.26$ deg (corrected), $R_e = 9 \times 10^6$].

ing scheme was 240×60 with 90 grid cells on the upper surface of the airfoil. The predicted lift coefficient is 0.346. The experimental value for the normal coefficient is 0.390. An examination of the γ'_{pu} values predicted by the present model in Fig. 3 reveals that the model was switched completely to the separated formulation (i.e., $\gamma'_{pu} \leq 0.5$) in the range $0.53 \leq x/c \geq 0.83$. This is also the extent of the separation bubble predicted for this case.

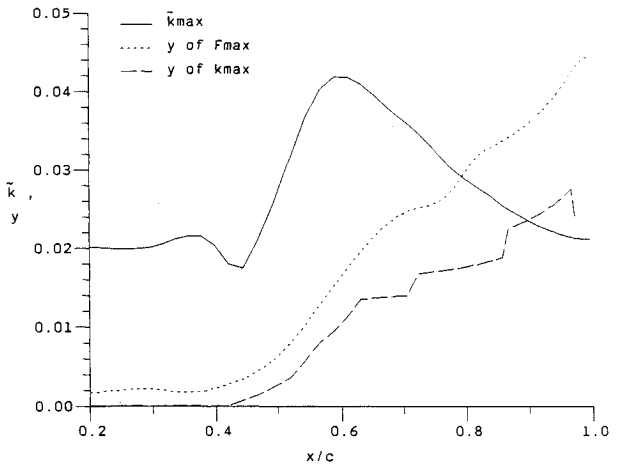

Fig. 4 Computed $\tilde{k}_{max}$, y_{Fmax}, and y location of $\tilde{k}_{max}$ distributions on upper surface of an NACA 0012 airfoil [$M_\infty = 0.799$, $\alpha = 2.26$ deg (corrected), $R_e = 9 \times 10^6$].

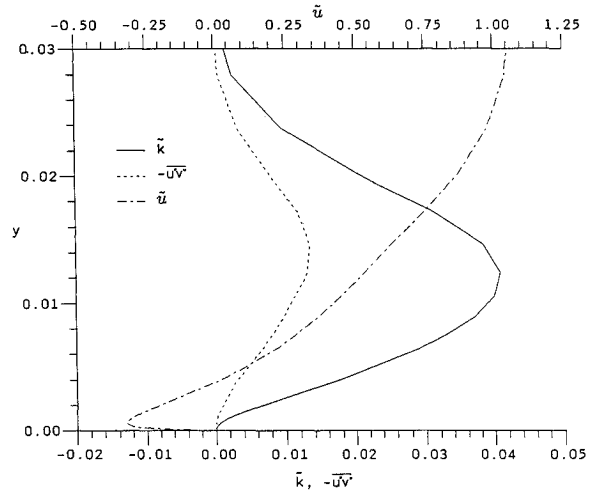

Fig. 5 Computed profiles of $\tilde{k}$, $-\overline{u''v''}$, and $\tilde{u}$ at $x/c = 0.63$ on upper surface of an NACA 0012 airfoil [$M_\infty = 0.799$, $\alpha = 2.26$ deg (corrected), $R_e = 9 \times 10^6$].

Figure 4 shows the streamwise variation of maximum $\tilde{k}$ and its location computed for this case. Also shown in the figure is the computed y_{Fmax} distribution used in the outer-layer length scale definitions. For attached flows, the maximum $\tilde{k}$ is near the wall. For strong adverse pressure gradient and separated flows, the location of $\tilde{k}_m$ moves away from the wall. In the separation region where the boundary layer thickens rapidly, there is also an increase in the turbulent kinetic energy. Figure 5 shows the computed streamwise velocity, turbulent kinetic energy, and Reynolds shear stress profiles in the separated region ($x/c = 0.63$). The maximum $\tilde{k}$ location is well above the backflow region almost to the middle of the boundary layer. The figure also shows that the Reynolds shear stress is near zero near the wall. Both of these characteristics are observed in Simpson's measurements of separated flow.

Two RAE 2822 airfoil cases are examined next. Both cases use a 418×80 grid with 240 cells on the airfoil's upper surface and 80 cells on the lower surface. The grid extent is 20 chords in all directions. The normal spacing of the first point off the wall is 1×10^{-5}. The first case is $M_\infty = 0.73$, $R_e = 6.5 \times 10^6$ flow at corrected $\alpha = 2.8$ deg (case 9 of Ref. 14). This transonic case has a moderately strong shock on the upper surface. Figure 6a compares the computed pressure distribution with the experimental data of Ref. 14 and Coakley's results using the Johnson-King model. Figure 6b compares the computed pressure distribution with the

experimental data and Coakley's results using the Baldwin-Lomax turbulence model and the two-equation q-ω model. Although the algebraic model, the two-equation model, and the present one-equation model predict the shock location and strength close to the experimental values, the Johnson-King model predicts a shock location upstream of the measured location. The present model predicts a lift coefficient for this case of 0.796. The experimental value for the normal coefficient is 0.803. Figure 7 compares the same group of model's skin-friction results with the experimental data. The present one-equation model predicts skin-friction values above both the experimentally measured values and the values predicted by the other turbulence models. Only the Baldwin-Lomax turbulence model predicts shock-induced separation.

Next, the RAE 2822 airfoil at $M_\infty = 0.75$, $R_e = 6.2 \times 10^6$, and corrected $\alpha = 2.4$ deg was examined (case 10 of Ref. 14). Figures 8a and 8b compare the computed pressure distribution with the other turbulence models and the experimental data. This case involves a strong shock on the upper surface. As in the NACA 0012 case with a strong shock, the algebraic model, the present one-equation model and two-equation model predict a shock location which is too far downstream, where as the Johnson-King model predicts the shock location accurately. Figure 9 compares the skin-friction results. The life coefficient is predicted to be 0.735 by the present model. The experimental value is 0.743 for the normal coefficient. The Johnson-King and the Baldwin-Lomax model predict shock-induced separation. In the present model's calculation, examination of the γ'_{pu} distribution reveals that the separated formulation is engaged in a small region behind the shock, although no mean backflow results.

In summary, the current formulation presents a possible framework for modeling separated turbulent flows. However, it is clear from the above results that the model in its present form still suffers a number of limitations. It is believed that the attached-flow formulation and the γ_{pu} blending function have sound physical basis. Thus, the deficiencies and limita-

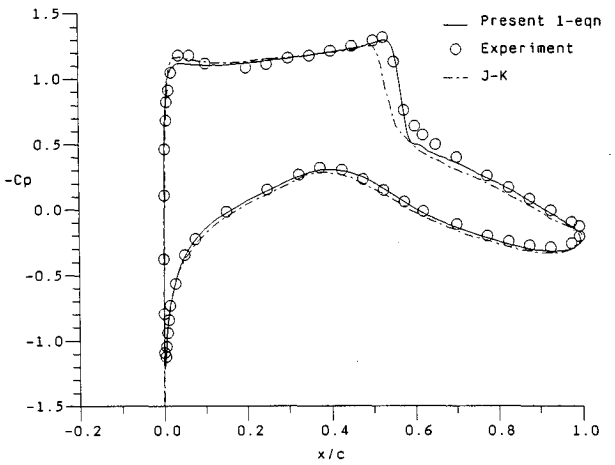

Fig. 6a Turbulent flow over the RAE 2822 airfoil [case 9: $M_\infty = 0.73$, $\alpha = 2.8$ deg (corrected), $R_e = 6.5 \times 10^6$]: pressure distributions.

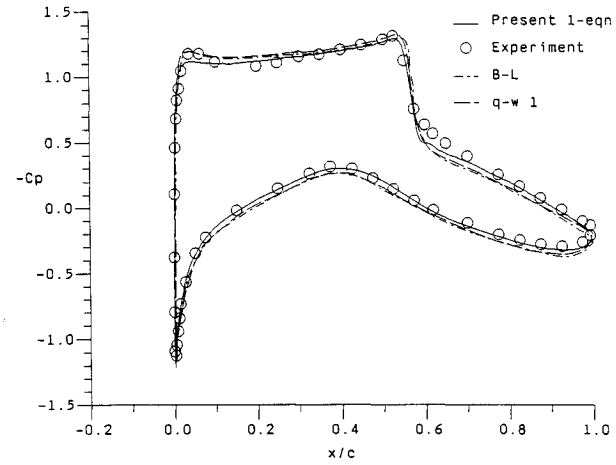

Fig. 6b Turbulent flow over the RAE 2822 airfoil [case 9: $M_\infty = 0.73$, $\alpha = 2.8$ deg (corrected), $R_e = 6.5 \times 10^6$]: pressure distributions.

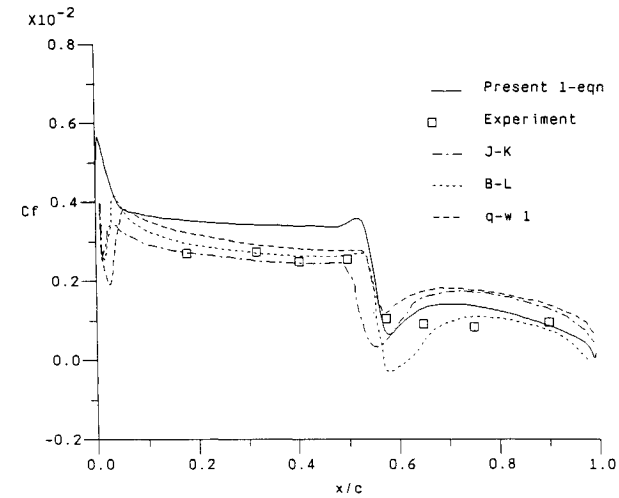

Fig. 7 Turbulent flow over the RAE 2822 airfoil [case 9: $M_\infty = 0.73$, $\alpha = 2.8$ deg (corrected), $R_e = 6.5 \times 10^6$]: upper surface skin-friction comparisons.

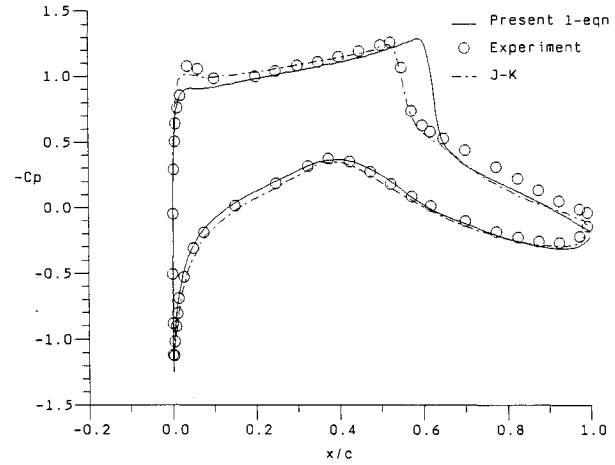

Fig. 8a Turbulent flow over the RAE 2822 airfoil [case 10: $M_\infty = 0.75$, $\alpha = 2.4$ deg (corrected), $R_e = 6.2 \times 10^6$]: pressure distributions.

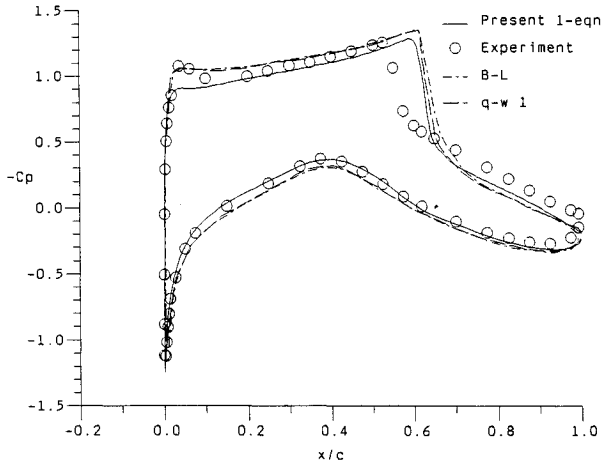

Fig. 8b Turbulent flow over the RAE 2822 airfoil [case 10: $M_\infty = 0.75$, $\alpha = 2.4$ deg (corrected), $R_e = 6.2 \times 10^6$]: pressure distributions.

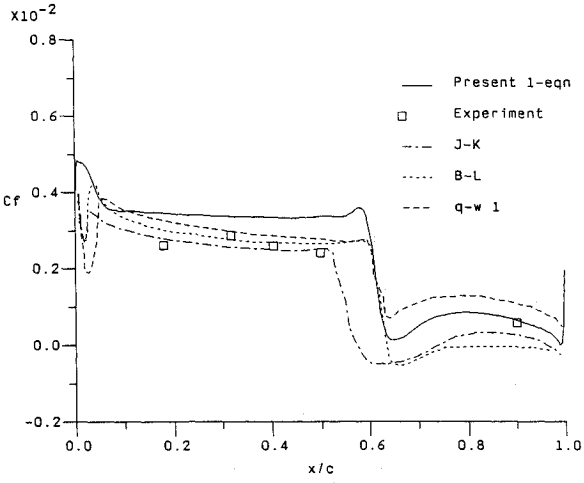

Fig. 9 Turbulent flow over the RAE 2822 airfoil [case 10: $M_\infty = 0.75$, $\alpha = 2.4$ deg (corrected), $R_e = 6.2 \times 10^6$]: skin-friction comparisons.

tions are a result of inadequate formulation in the separated flow region. It is not possible to determine with certainty the causes of these limitations. However, the following factors present some serious candidates.

It has been suggested by Simpson[1] that the eddy viscosity assumption is not valid in the separated flow region. However, the available experimental data is not sufficient to reveal an alternative. After a number of futile attempts to establish an alternative correlation for the Reynolds stresses, the present effort was forced to retain the eddy viscosity assumption. Next, the modeled form of the turbulent energy equation utilized does not contain constitutive terms for the pressure-work and pressure-diffusion effects. Judging by the model's incorrect prediction of shock location for separated flows, it would appear that appropriate modeling of these terms in the turbulent energy equation is important. Furthermore, the choice of length scales for the separated-flow formulation were based on the Schofield-Perry similarity profile for the forward flow region above the backflow region. This similarity relation has limitations. Again, lack of adequate data prevented a more general correlation.

The preceding results presented were computed on a CRAY 2 supercomputer. The present model requires the solution of only one additional equation and the computation of algebraic length scales. Computationally, the model should "cost" less than the two-equation models and no more than the Johnson-King model which Johnson and King[4] report to cost 37% more than Baldwin-Lomax.

Conclusions

A one-equation turbulence model based on the turbulent kinetic energy equation is presented. The model is developed directly from the available experimental observations of both attached and separated flows. The model does not require prior knowledge of separation or its location. Starting directly from freestream initial conditions, it can be used to calculate flows past a flat plate, attached, and separated airfoil cases without adjustments.

Based on the results obtained, the model duplicates the success of algebraic models in attached-flow cases. For separated-flow cases, it predicts shock location and strength closer to the experimentally observed values than both the algebraic and two-equation models. However, when predicting shock location for cases with shock-induced separation, the model suffers some limitations due to either errors in the separated-flow formulation of the model or the modeled form of the turbulent kinetic energy equation being solved.

Acknowledgments

This work is supported in part by the following grants: NASA Cooperative Agreement NCCI-22; the Hypersonic Aerodynamics Program Grant NAGW-1022 funded jointly by NASA, Air Force Office of Scientific Research, and Office of Naval Research; and the Mars Mission Center funded by NASA Grant NAGW-1331. The authors would like to express their appreciation to Roger Simpson for providing us with his tabulated measurement and to Charles Swanson for allowing us to use his 1984 Navier-Stokes code. H. A. Hassan would like to acknowledge helpful discussions with Roger Simpson and Tom Coakley.

References

[1]Simpson, R. L., "Two-Dimensional Turbulent Separated Flow," AGARDograph No. 287, Vol. 1, 1985.

[2]Patel, V. C., Rodi, W., and Scheuerer, G., "Turbulence Models for Near Wall and Low-Reynolds-Number Flows: A Review," *AIAA Journal*, Vol. 23, Sept. 1985, p. 1308.

[3]Coakley, T. J., "Numerical Simulation of Viscous Transonic Airfoil Flows," AIAA Paper 87-0416, Jan. 1987.

[4]Johnson, D. A., and King, L. S., "A Mathematically Simple Turbulence Closure Model for Attached and Separated Turbulent Boundary Layers," *AIAA Journal*, Vol. 23, Nov. 1985, pp. 1684–1692.

[5]Baldwin, B. S., and Lomax, H., "Thin-Layer Approximation and Algebraic Model for Separated Turbulent Flows," AIAA Paper 78-257, Jan. 1978.

[6]Schofield, W. H., "Two-Dimensional Separating Turbulent Boundary Layers," *AIAA Journal*, Vol. 24, Oct., 1986, pp. 1611–1620.

[7]Swanson, R. C., and Turkel, E., "A Multistage Time-Stepping Scheme for the Navier-Stokes Equations," ICASE Rept. No. 84-62, Feb. 1985.

[8]Rebesin, M. W., and Rose, W. C., "The Turbulent Mean-Flow, Reynolds-Stress, and Heat-Flux Equations in Mass-Averaged Dependent Variables," NASA TM-X-62248, March 1973.

[9]Launder, B. E., Reece, G. J., and Rodi, W., "Progress in the Development of a Reynolds Stress Closure," *Journal of Fluid Mechanics*, Vol. 68, Oct. 1975, p. 537.

[10]Hinze, J. O., *Turbulence*, 2nd ed., McGraw-Hill, New York, 1975.

[11]Wolfstein, M., "The Velocity and Temperature Distribution in One-Dimensional Flow with Turbulence Augmentation and Pressure Gradient," *International Journal of Heat and Mass Transfer*, Vol. 12, Dec. 1969, pp. 301–318.

[12]Chen, H. C., and Patel, V. C., "Practical Near-Wall Turbulence Models for Complex Flows Including Separation," AIAA Paper 87-1300, June 1987.

[13]Thibert, J. J., Granjacques, M., and Ohman, L. H., "NACA 0012 Airfoil," Experimental Data Base for Computer Program Assessment, AGARD Advisory Rept. No. 138, May 1979.

[14]Cook, P. H., McDonald, M. A., and Firmin, M. C. P., "AEROFOIL RAE 2822 Pressure Distributions, Boundary-Layer and Wake Measurements," AGARD Advisory Rept. No. 138, 1979.